Fluorescence-based assays to analyse phosphatidylinositol 5-phosphate PI(5)P in autophagy

Mariella Vicinanza[1], Matthew J Gratian[1], Mark Bowen[1], David C Rubinsztein[1*]

Department of Medical Genetics, Cambridge Institute for Medical Research, Wellcome/MRC Building, Cambridge Biomedical Campus, Hills Road, Cambridge, CB2 0XY, UK

Corresponding author: dcr1000@cam.ac.uk

Contents

Abstract

Autophagosome formation is stimulated by VPS34-dependent PI(3)P formation and by alternative VPS34-independent pathways. We recently described that PI(5)P regulates autophagosome biogenesis, and rescues autophagy in VPS34-inactivated cells, suggesting that PI(5)P contributes to canonical autophagy. Our analysis revealed a hitherto unknown functional interplay between PIKfyve and PIPK type II in controlling PI(5)P levels in the context of autophagy. Among phosphoinositides, visualization of PI(5)P in intact cells has remained difficult. While PI(5)P has been implicated in signalling pathways, chromatin organization, bacterial invasion and cytoskeletal remodelling, our study is the first report showing PI(5)P localization on autophagosomes and early autophagosomal structures when autophagy is induced by nutrient deprivation (amino acids or glucose starvation). We provided a detailed analysis of PI(5)P distribution by the use of Super Resolution Structured Illuminated microscopy. Here we present a set of tools for detection of PI(5)P during autophagy by confocal microscopy, live-cell imaging, and Super Resolution microscopy.

Keywords: autophagy, PI(5)P, Super Resolution Structured Illumination microscopy

1. PI(5)P role in autophagy

Phosphoinositides (PIs) are low-abundance lipids that cluster on cytosol-facing platforms to dynamically recruit effector proteins to specific membranes (Balla 2013). The metabolism of PIs is locally regulated by sets of phosphoinositide kinases and phosphatases distributed in diverse intracellular compartments. Their inter-

convertibility enables PIs to undergo rapid changes in response to nutrient availability and cell stress, and makes PIs ideal transducers of perturbations of cellular homeostasis and metabolism into membrane trafficking events.

First identified in 1997 (Rameh, Tolias et al. 1997), PI(5)P has been implicated in growth factor signalling pathways (Liu, Liu et al. 2006, Boal, Mansour et al. 2015), chromatin organization and gene expression (Di Lello, Nguyen et al. 2005, Alvarez-Venegas, Sadder et al. 2006, Viiri, Janis et al. 2009, Gelato, Tauber et al. 2014, Stijf-Bultsma, Sommer et al. 2015), bacterial invasion and cytoskeletal remodelling (Grindheim, Hollas et al. 2014, Viaud, Lagarrigue et al. 2014). PI(5)P levels have been shown to increase in response to stimuli such as thrombin, insulin, oxidative and osmotic stress, etoposide and UV irradiation, cell cycle progression, fibroblast growth factor 1 (FGF1) (Viaud, Boal et al. 2014). PI(5)P production is relevant to infections with Salmonella and Shigella flexneri (Niebuhr, Giuriato et al. 2002), T cell activation and antiviral innate immune responses (Guittard, Gerard et al. 2009, Guittard, Mortier et al. 2010), myogenic differentiation (Fugier, Klein et al. 2011, Stijf-Bultsma, Sommer et al. 2015) and carcinogenesis (Viaud, Boal et al. 2014).

Autophagy is a bulk degradation process that delivers cytosolic content to lysosomes, and is induced by stress conditions like nutrient deprivation, growth factor withdrawal and low cellular energy levels (Rubinsztein, Codogno et al. 2012). The double-membraned autophagosomes are formed from cup-shaped, double-membrane precursors, called phagophores, whose edges have not yet fused. Phagophores are positive for both LC3 and ATG16L1, while autophagosomes have LC3 but no ATG16L1 (see Figure 1a). Autophagy has been classically considered to be

phosphatidylinositol 3-phosphate (PI(3)P)-dependent. Genetic studies in yeast and flies and pharmacological manipulations in cells suggested that PI(3)P production by the class III phosphatidylinositol 3-kinase (VPS34) is required for autophagosome formation as this lipid enables the recruitment of proteins necessary for autophagosome biogenesis (like WIPI1-2, WD-repeat protein interacting with phosphoinositide) (Proikas-Cezanne, Takacs et al. 2015) (Dall'Armi, Devereaux et al. 2013). However, autophagosomes can be detected in T-lymphocytes and sensory neurons from *Vps34*$^{-/-}$ mice (Zhou, Wang et al. 2010) and in glucose-depleted cells treated with VPS34 inhibitors (Codogno, Mehrpour et al. 2012, McAlpine, Williamson et al. 2013), suggesting that a PI(3)P-independent, non-canonical autophagy pathway exists.

We recently reported a role for phosphatidylinositol 5-phosphate PI(5)P in autophagy (Vicinanza, Korolchuk et al. 2015). This is compatible with previous reports showing autophagy regulatory proteins binding PI(5)P (Lorenzo, Urbe et al. 2005, Baskaran, Ragusa et al. 2012). We detected PI(5)P on nascent and mature autophagosomes. Increased cellular PI(5)P levels enhanced autophagosome formation, while depletion of PI(5)P decreased the numbers of autophagosome precursors and completed autophagosomes. We found that elevating PI(5)P levels was able to induce autophagosome formation even when VPS34 was inhibited or silenced, leading us to conclude that PI(5)P can serve as an “alternative” to PI(3)P in the autophagosome biogenesis. We confirmed that PI(5)P is involved in PI(3)P-independent autophagy pathways like glucose starvation- or resveratrol-induced autophagy, where PI(3)P is dispensable (Figure 1A).

The levels of phosphoinositides are also important for autophagosome maturation. PI(3)P promotes retrograde movement of autophagosomes via the dynein–dynactin complex and its effector FYCO1 (FYVE and coiled-coil domain containing 1) (Pankiv, Alemu et al. 2010), while the completion of autophagy requires clearance of PI(3)P (via myotubularin 3-phosphatases) enabling fusion with the lysosome (Vergne and Deretic 2010). PI(3,5)P2 has been proposed to promote fusion events and compartment acidification at the endo-lysosomal network and promote recycling of autophagolysosome membrane (McCartney, Zhang et al. 2014).
Although PI(5)P has been reported to regulate endosome maturation, it remains undefined whether PI(5)P plays a role in autophagosome-lysosome fusion (Boal, Mansour et al. 2015).

2. Microscopy-based detection of PI(5)P

About 2% of the human genome encodes proteins carrying specific PI-binding domains (including PH, FYVE, PX, PHD domains) (Hammond and Balla 2015). These domains have become valuable tools in visualizing PIs in intact cells. When expressed as fusions with fluorescent probes (i.e. GFP, RFP), PI-binding domains can be used to determine the intracellular location and relative levels of PIs in live and fixed cells by wide-field or confocal fluorescent microscopy.
Note: Extreme care must be applied when PI-reporters are exogenously expressed in cells because, depending on the level of expression and the PI affinity of the probe, problems may occur like limited access to certain PIs pools that are already in complex with cellular proteins or interference of exogenous PI-domains that can prevent endogenous proteins from interacting with their cognate lipid.

A major limitation in studying the intracellular localisation of endogenous PI(5)P is its low abundance (estimated as approximately 1–2% of monophosphorylated PIs).

Several biochemical and microscopy approaches have detected PI(5)P pools at plasma-membrane, nucleus and endosomal compartments (Jones and Smirnoff 2006, Sarkes and Rameh 2010, Ramel, Lagarrigue et al. 2011). Another limitation in studying PI(5)P localization is the uncertain specificity of PI(5)P bio-probes. PI(5)P-binding proteins are beginning to be identified (Figure 1B) and include proteins carrying the PHD (plant homeodomain) finger, the PH (pleckstrin homology) domain, the PH-GRAM (Glucosyl transferase, Rab-like GTPase activator and Myotubularins) or PBR (PolyBasicRegion) motif (Figure 1B). The PHD domains are zinc-finger motifs and PHD finger of Inhibitor of Growth Protein 2 (ING2) was one of the first convincingly shown to interact with PI(5)P (Gozani, Karuman et al. 2003). The PHD domain of ING2 (Gozani, Karuman et al. 2003, Bua, Martin et al. 2013) and the PH domain of Dok (Downstream of Kinase) proteins (Guittard, Gerard et al. 2009, Guittard, Mortier et al. 2010) show strong preference for PI(5)P and have been used to obtain spatial information on the distribution of PI(5)P.

We detected PI(5)P using GFP-tagged PHD3X (three tandem repeats of PHD domain of ING2) on discrete puncta, which were positive for autophagosome markers and increased in numbers when cells were starved (Vicinanza, Korolchuk et al. 2015).
A PHD mutant defective in PI(5)P binding has been used as a control (PHD3X Znmut) (Bua, Martin et al. 2013). It is critical to avoid extreme PHD3X overexpression, as overexpression (30 hours) of GFP-PHD3X (and GFP-PH-Dok-5) sequester intracellular PI(5)P and dramatically decrease the number of mature autophagosomes appearing in starved-cells.

2.1 Cell culture conditions

We grow HeLa, human cervix, adenocarcinoma (ATCC, CCL-2) at 37°C and 5% CO2 in Dulbecco's Modified Eagles Medium (DMEM) with 4500 mg/l glucose, sodium pyruvate (1 mM) (Gibco/Invitrogen Corporation), supplemented with L-Glutamine (2mM), 10% fetal calf serum (FCS) (Sigma), 100 U/ml penicillin, and 100 mg/ml streptomycin solution (Gibco/Invitrogen Corporation). We routinely use 75 cm^2 BD Falcon Culture Flasks with 0.2 mm Vented Blue Plug Seal Cups (BD Europe, France). For long-term storage in liquid nitrogen, we freeze 1-5 X 10^6 cells in 2 ml of FCS 10% Dimethyl-sulfoxide (DMSO). We routinely check for the absence of mycoplasma by PCR analyses.

Generally, we seed 1–2 × 10^5 cells in 2 ml of culture medium on glass coverslips in each well of BD Falcon 6-well tissue culture plates (BD Falcon, Europe, France). Transfection was performed with TransIT 2020 Mirus (for DNA) or LipofectAMINE 2000 (for siRNA) reagents (Invitrogen), using the manufacturer's protocol.

Autophagy induction by nutrient deprivation:

Amino-acid and serum deprivation: cells incubated in Hanks balanced salt solution (HBSS) media (Invitrogen) for 1-2 hours (*note*: HBSS does not contain amino-acids and serum and does contain low levels of glucose: 1g/l of D-glucose versus 4.5 g/l glucose in DMEM); Glucose deprivation: cells incubated in DMEM lacking glucose (Invitrogen, #11966) with 10% dialyzed FBS (Sigma) and glutamine for 4-6 h.

2.2 Autophagosomal markers

Mature autophagosomes and autophagolysosomes can be detected using RFP-LC3B transiently expressed in HeLa cells for 16 h. Phagophores and pre-phagophore structures can be detected using mStrawberry-ATG16L1 transiently expressed in

HeLa cells for 16 h (Ravikumar, Moreau et al. 2010). In both cases, care needs to be taken to avoid overexpression artefacts. To better visualize phagophores we use the expression of proteolytic activity-deficient mutant of ATG4B (ATG4BC74A). This is tool that freezes the phagophore stage (that in normal conditions are transient and rare structures) by preventing LC3 lipidation and autophagosome completion (Fujita et al., 2008).

2.3 Expression of GFP-PHD3X(ING2) to visualize PI(5)P during autophagy by confocal microscopy

1. HeLa cells were seeded at 1–2 × 10^5 cells in 2 ml of culture medium on glass coverslips in 6 well plates. Cells were incubated overnight to 70-80 % confluency at 37°C and 5% CO_2.
2. Place 200 μl of pre-warmed OPTIMEM reduced-serum medium in a sterile tube under the hood.
3. Add 1 μg of GFP-PHD3X (or GFP-PHD3X Znmut as negative control) and 0.3 μg of ATG16L1-mStrawberry/ 0.5 μg of RFP-LC3 to 200 μl OPTIMEM by gently pipetting (*Note*: in cases of triple transfection, we used 0.8 μg of GFP-PHD3X, 0.3 μg of ATG16L1-mStrawberry and 0.5 μg of flag-tagged ATG4B (ATG4BC74A)).
4. Briefly vortex transfection reagent TransIT 2020 Mirus (Invitrogen) at room temperature and then add 3-4 μl of Mirus to the diluted DNA mixture. (*Note*: We usually keep a DNA:Mirus ratio of 1:3).
5. Pipette gently to mix and incubate at room temperature for 15-20 min, with mixing every 5 min.
6. Slowly apply the 200 μl Mirus-DNA complex to wells by gently pipetting

into 1 ml full serum culture media (*Note*: before adding transfection complex, cells were washed in complete culture medium containing 10% serum and low levels of antibiotics).

7. Incubate cells for 16 hours.
8. Aspirate off the full serum culture medium, wash twice with pre-warmed HBSS (37°C) to remove residual serum and incubate with 1 ml of pre-warmed HBSS (37°C) for 1 hour.
9. Fix the cells adding 1ml of pre-warmed 4% paraformaldehyde (dissolved in PBS, pH 7.0 freshly made a few hours earlier from powder) to 1 ml of HBSS (final concentration is 2% paraformaldehyde) and incubate for 10 min at room temperature.
10. Wash the cells 2 times with PBS and once with water.
11. Coverslips are mounted with 20µl ProLong Antifade Reagent (Molecular Probes, catalog number P-36930) and stored at 4°C in the dark.

For confocal laser scanning microscopy, we used LSM710 and LSM780 microscopes (Zeiss). All images were taken with 63X 1.4NA DIC Plan-Apochromat oil-immersion objectives (Zeiss, Jena). We currently use helium neon lasers for excitations at 543 or 633 nm, a diode laser for excitation at 561nm and argon lasers for excitations at 488 nm. As a standard procedure, we take 8-10 fields, enough to collect images from about 80 cells for each condition and then we also acquire higher magnification images of 5 individual cells.

Any saturated images identified by using the integrated Range Indicator tool are discarded and acquisition settings (i.e. laser intensity) are adjusted accordingly.

ImageJ is used for further analysis (number of vesicles analysis and colocalisation) and processing of confocal images.

3. Manipulations of PI(5)P levels to visualize PI(5)P during autophagy

Manipulation of intracellular PI(5)P levels by targeting enzymes relevant for its biogenesis and turnover showed that GFP-PHD3X puncta formation under autophagy induction conditions is dependent on PI(5)P (Vicinanza, Korolchuk et al. 2015). PI(5)P biosynthesis is regulated by the type III PtdInsP 5-kinase PIKfyve as reduced PI(5)P levels are seen in PIKfyve hypomorph and heterozygous mice and in cells silenced by siRNA, overexpressing a dominant-negative, or treated with pharmacological inhibitor of the kinase (Sbrissa, Ikonomov et al. 2002, Ikonomov, Sbrissa et al. 2011, Sbrissa, Ikonomov et al. 2012, Zolov, Bridges et al. 2012).

PIKfyve can either directly phosphorylate PI, or make PI(3,5)P2, which is then transformed into PI(5)P by 3-phosphatases of the myotubularin family (MTMRs) (Figure 1c). On the other hand, the major route for PI(5)P removal is attributed to type II PIPK kinases (phosphatidylinositol 5-phosphate 4-kinases, PI5P4K) (Clarke, Wang et al. 2010, Shisheva 2013, Viaud, Boal et al. 2013).

Although we cannot exclude that the PHD3X domain binds other lipids (mainly PI(3)P) in addition to PI(5)P, PHD3X localized in our experiments at the nucleus and plasma-membrane, as previously described for PI(5)P (Jones and Smirnoff 2006, Sarkes and Rameh 2010). PHD3X detected PI(5)P on autophagosomes when PI(3)P levels where diminished (VPS34 inhibition by wortmannin treatment or 3-phosphatase MTMR3 overexpression), while PHD3X-positive structures were lost in conditions expected to increase PI(3)P levels but decrease PI(5)P levels (PIKFyve and

MTMR3 silencing) (Figure 1c). These observations lead us to conclude that PHD3X detects PI(5)P independently of PI(3)P, at least in autophagy-inducing conditions (HBSS or glucose-depleted media).

3.1 siRNA transfection

1. Routinely, two rounds of knockdown for 5 days with final siRNA concentrations of 50 or 100nM are applied.
2. Seed HeLa cells at 60-70% confluency in 6 well plates and incubate overnight to at 37°C and 5% CO_2.
3. Day 1: dilute 5-10 μl Lipofectamine 2000 (Invitrogen, catalog number 11668019) in 250 μl of pre-warmed OPTIMEM reduced-serum medium (Invitrogen, catalog number 51985042). Dilute 5-10 μl of siRNA oligos (stock solution 20μM) in 250 μl of pre-warmed OPTIMEM. Incubate for 5 min at room temperature. Combine diluted siRNA and diluted Lipofectamine 2000 and incubate 20 min at room temperature. Wash the cells with 1 ml of OPTIMEM and slowly apply the siRNA/Lipofectamine 2000 mixture (finale volume of 500 μl). Incubate for 6 hours at 37°C and 5% CO_2 and then replace the transfection medium with culture medium containing serum.
4. Day 2: repeat the siRNA oligo transfection.
5. Day 3: split cells and seed 1–2 × 10^5 cells in 2 ml of culture medium on glass coverslips in 6 well plates.
6. Day 4: Transfect cells with GFP-PHD3X in combination with RFP-LC3 or ATG16L1-mStrawberry (see section 2.3).
7. Day 5: incubate with 1 ml of pre-warmed HBSS (37°C) for 1 hour, fix and process for confocal microscopy (see section 2.3).

3.2 Genetic perturbation of PI(5)P levels

Decreased PI(5)P synthesis: PIKfyve (Gene ID: 200576) and MTMR3 (Gene ID: 8897) silencing;

Decreased PI(5)P removal: PIP4K2A (Gene ID: 5305), PIP4K2B (Gene ID: 8396) and PIP4K2C (Gene ID: 79837) silencing.

See Table 1 for siRNA oligos used (Dharmacon).

3.3 Pharmacological manipulations of PI(5)P

PIKfyve inhibitors: YM-201636 (Cayman Chem).

Incubate cells with 1 ml of fresh culture medium or HBSS or glucose-depleted medium containing 100 nM YM-201636 (*note*: we use low doses of YM-201636, between 100 nM and 200 nM, previously shown to selectively inhibit PI(5)P synthesis via PIKfyve (Sbrissa, Ikonomov et al. 2012)).

3.4 Fluorescent PI(5)P analogs

Fluorescently-labelled PI(5)P analogues are commercially available and include acyl-labelled BODIPY derivatives of PI(5)P. BODIPY (4,4-difluoro-3a,4a- diaza-s-indacene) is an hydrophobic fluorescent compound that, when attached to the end of one of the acyl chain (sn-1 position), can be used to monitor the distribution of PI(5)P without altering the structure of the inositol head group. BODIPY fluorescent analogs exist as FL (Excitation: 503nm/ Emission:513 nm) and TMR (Excitation: 542nm/ Emission:574 nm) versions (Echelon Bioscience, C-05F6a and C-05M6 respectively). BODIPY-PI(5)P analogues are loaded into cellular membranes with use of a specific carrier (Ozaki, DeWald et al. 2000).

We use BODIPY-PI(5)P di-C6 at final concentrations of 1 or 10 μM; carrier-only is

used as negative control. Cells are processed for live cell imaging, since BODIPY-PI(5)P analogs are not fixable. (Note: phosphoinositides cannot be fixed by standard fixatives and fixed cells cannot be permeabilized with standard detergents that may extract the lipids).

Cautionary note: use low adherent polystyrene tubes or glass tubes; reconstitute phosphoinositides and carriers in aqueous solution containing small amounts of methanol, ethanol or tert-BuOH; vortex mix and briefly sonicate to completely dissolve carriers and phosphoinositides; avoid using phosphate buffers when combining carrier and lipids.

3.4.1 Addition of exogenous PI(5)P to cells

1. BODIPY-labelled PI(5)P di-C6 and carrier (Echelon Bioscience) are reconstituted in H2O:tert-BuOH (9:1) solution.
2. Vortex for 1 min and apply 1 min of bath sonication (4°C, cold room) to reconstitute solutions.
3. Combine carrier and lipids at a 1:1 ratio in sterile low adherent tubes and incubate for 10 min at room temperature.
4. Dilute the mixture in starvation medium (HBSS) and use for short incubations (30 min to 1 hour) on cells.

3.4.2 Live cell imaging of cells loaded with fluorescent PI(5)P analogs

HeLa cells transfected with RFP-LC3 (see section 2.3) were exposed to HBSS containing BODIPY-labelled-PI(5)P for 1h and followed by live cell imaging for 10 min in pre-warmed buffered HBSS medium (10 mM Hepes).

We performed time-lapse microscopy using a Zeiss LSM 780 confocal microscope

equipped with 488nm argon, 561nm diode and 633nm HeNe lasers and a 63X 1.4NA DIC Plan-Apochromat oil immersion objective (Carl Zeiss, Jena, Germany). The microscope was operated using the ZEN black software, version 2012. To allow live cell imaging, the microscope was equipped with a PeCon XL3 environmental chamber, temperature control unit and heating unit (Zeiss, Jena)

To prepare for time-lapse microscopy, HeLa cells are grown to 70% confluency in 35mm MatTek glass bottom dishes (MatTek Corporation, Ashland, MA), transfected with RFP-LC3 (see section 2.3) and loaded with fluorescent PI(5)P (see section 3.4.1).

The incubator is equilibrated to 37°C before starting the time-lapse microscopy. Images were taken at interval of 10 seconds for 10 min. Images series were elaborated by using ImageJ software.

4. Super-Resolution Structured Illumination Microscopy (SR-SIM) to visualize PI(5)P during autophagy

Conventional light microscopy (i.e. confocal) is useful to determine whether a given phosphoinositide is enriched on a specific organelle but does not allow discrimination between closely adjacent small membrane compartments or membrane subdomains. In this respect, electron microscopy (EM) provides a much higher resolving power than standard light microscopy; however fixation and post-fixation manipulations required can potentially affect the structure of lipids. Super-resolution microscopy provides resolution between conventional light microscopy and EM. Conventional light microscopy, including confocal, is subject to optical diffraction which places a physical limit on the resolution achievable. This limit is approximately half the

wavelength of the emitted light and is often generalized to be 200nm maximum. In recent years various techniques and technologies have been used to circumvent this limit and thereby achieve so-called super-resolution.

We carried out 3D analysis of GFP-PHD3X-labelled structures by Super-Resolution Microscopy using a Zeiss Elyra PS1 microscope, in order to have a deeper understanding of PI(5)P localization on nascent autophagosomes in autophagy-stimulating-conditions (amino-acid and serum starvation, HBSS media) (Vicinanza, Korolchuk et al. 2015) (Figure 3).

4.1 Super-resolution Structured Illumination Microscopy (SR-SIM)

Super-resolution Structured Illumination Microscopy (SR-SIM) is a technique which allows extraction of normally unresolvable high-frequency information by means of a moving pattern in the illuminating light coupled with post-acquisition computational reconstruction of multiple images into a single super-resolved image or volume. By super-imposition of a known pattern (the illumination) onto an unknown pattern (the details of the sample), followed by careful analysis of the interference between the two patterns, extraction of detail beyond the resolving power of the objective is achieved.

The structured illumination pattern in the Zeiss Elyra is formed by inserting a grid into the incident light-path which projects a regular arrangement of light and dark stripes into the sample. The pattern spacing is tailored to the wavelength(s) required and is shifted in both phase and rotation during the acquisition of multiple images.

SR-SIM offers two main advantages over confocal imaging, a 2-fold increase in resolution in x,y and z dimensions and a large increase in dynamic range. For example, the 250nm conventional resolution for GFP is increased to 125nm laterally and around 250nm axially. This 2-fold increase in x,y and z resolution equates to an 8x reduction in the size of the smallest imaging volume (Gustafsson, *et al*., 2008) (Figure 2a and 2c).

SR-SIM is a widefield technique making use of cameras (typically sCMOS type), which results in a large increase in dynamic range vs. confocal microscopes using PMT (photomultiplier type) detectors, therefore more weakly fluorescent structures are easily detected without the risk of saturation of brighter structures. Thus, SR-SIM images routinely demonstrate a much larger population of fluorescent structures than can be observed in a single confocal image.

The main disadvantage of SR-SIM is the speed of acquisition. In order to generate one super resolved optical section in a single colour, it is necessary to collect a minimum of 5 grid phases and 3 grid rotations, ie. a minimum of 15 images (Figure 2c). Resolution isotropy is improved by increasing the number of grid rotations captured up to 5, resulting in 25 images per colour per optical section. Imaging is therefore necessarily slow and this greatly reduces its applicability for live samples. If structures in the sample move during the acquisition of the multiple images required for capture of a single time point, then the reconstruction algorithms will give rise to artefacts. Recently, this speed issue has been addressed by the use of very rapid imaging techniques using light-sheet illumination and spatial light modulators to

generate the SIM pattern. These instruments bring SR-SIM into the realm of rapid live cell imaging (Chen, Legant et al. 2014).

4.2 Instrument preparation

For SR-SIM, we use a Zeiss Elyra PS1 (Carl Zeiss GmbH, Jena, Germany. http://www.zeiss.com/microscopy/en_de/products/superresolution-microscopy.html) (Figure 2b) with a carefully matched 63x 1.4NA Zeiss Plan-Aprochmat objective. This lens was specially selected from a batch to produce an optimally formed point-spread function (psf) on our particular instrument.

1. **Stabilization**: In order to maximise system stability and compensate for environmental variations, the microscope is sited on an active anti-vibration table (Vision IsoStation, Newport Corp. Irvine. CA) and is isolated with an environmental chamber (PeCon GmbH, Jena, Germany). This chamber also provides additional laser safety interlocks and is black to prevent the transmission of harmful laser radiation.
2. **Temperature**: We maintain the room temperature at around 18-20°C during imaging and heat the environmental chamber to precisely 23°C which produces the optimal refractive index in the immersion oil (Immersol 1.518 at 23°C, Carl Zeiss GmbH, Jena). Slides and oil are stored in the chamber so the entire optical train is at 23°C.
3. **Stage Equilibration/thermal alignment**: The Elyra instrument is allowed to equilibrate for at least 3 hours after switching on, to stabilise the focus (ie, to minimise expansion/contraction of elements forming the optical path). Subsequent to this equilibration, the stage insert is aligned so that it is exactly perpendicular to the optical light path through the objective. This is achieved

by means of two set-screw adjustments on the stage insert which are turned to super-impose two reflected images using a custom made alignment tool.

4. **Chromatic aberration correction**: After stage alignment and thermal equilibration, it is necessary to perform a bead alignment to correct for any chromatic aberration which may be present. Chromatic aberration, which arises from imperfections in the optical system, would be too small an effect to be problematic in confocal imaging but is resolvable by super-resolution instruments; it manifests as a mismatch in the alignment of the different colour channels. For example, different colours will be offset from one another to some degree. By imaging multi-colour fluorescent beads (2076-515 Low Density MultiSpec, Carl Zeiss GmbH, Jena), this mismatch can be quantified and a table of corrections generated using an affine analysis method. These corrections, which include lateral and axial offsets, image rotations and shear in all 3 dimensions, are saved as an alignment calibration file and are subsequently used to correct the experimental images. Thus, we can ensure that structures which colocalize to within the resolution of the Elyra are correctly presented as colocalized.

4.3 Sample preparation

1. HeLa cells were seeded at 1–2 × 10^5 cells in 2 ml of culture medium on high-precision 18mm square number 1.5 coverslips (Zeiss ltd) (which have a thickness of 170μm and a variation of less than +/- 5μm) in 6 well plates. Cells were incubated overnight to 70-80 % confluency at 37°C and 5% CO2.
2. Cells were transfected with 0.3 μg of ATG16L1-mStrawberry (or RFP-LC3) and 1 μg of GFP-PHD3X (section 2.3).

3. Coverslips are mounted with 20µl ProLong Gold (P36934, LifeTechnologies) and allowed to cure at room temperature for 72 hours in order to achieve a refractive index which matches the immersion oil at 23°C. These coverslips are mounted on conventional glass slides without frosting or adhesive labels, in the geometric centre, one coverslip per slide. Note: If single side frosted slides are used, it is important to mount the coverslip on the plain side so that it will lie completely flat on the microscope stage. Slides frosted on both sides should not be used.

4.4 Sample Imaging

The slides are pre-heated to 23°C by placing them in the microscope chamber for 10 minutes before imaging.

Image Acquisition: Images are acquired with the following microscope configuration. Excitation of the three channels is by 488nm/200mW, 560nm/200mW and 640nm/150mW diode lasers, structured illumination grid pitches are 28um, 34um and 34um, respectively, and emission filters are BP495-550, BP570-620 and LP655nm. We image z-stack through-focus series of images at a spacing interval of 110nm in 3 colours sequentially using 5 grid phase shifts and 5 grid rotations, resulting in a raw data image sequence comprising 75 images per z-slice. A typical z-stack comprises of 20 slices covering an approximately 2µm thickness of the sample, thus resulting in 1,500 images total per single output volume. The camera used is a PCO edge sCMOS device (PCO AG, Kelheim, Germany), which is thermoelectrically cooled to 5°C. Waste heat is extracted with a liquid cooling system (Innovatak OS GmbH, Stammham, Germany) to prevent the vibrations, which occur with fan-based camera cooling. This camera has a large area sensor and is capable of imaging up

2240x2154 pixels but this is typically not necessary, as 1024x1024 or 512x512 usually provide an ample field area. 512x512 pixels equates to a field area of 52.7μm^2. Raw data in the form of multi-dimensional image arrays are processed in the frequency domain using complex reconstructive algorithms (Gustafsson, Shao et al. 2008).

We have found that as long as the sample is prepared optimally and the correct materials are used to maintain consistency of refractive index, the automated structured illumination processing built into the Elyra version of ZEN software performs extremely well. Adjustment of manual processing parameters is possible for 'difficult' samples such as particularly thick specimens, low signal to noise ratio or (to some extent) refractive index mismatch. However, we have found that it is far better to optimise the sample preparation than to adjust the image processing parameters. If the structured illumination pattern is not visible during imaging due to inadequate matching of refractive index, no amount of post-processing will generate an acceptable super-resolved image.

4.5 Image processing

Reconstructed images are then corrected for spherical and chromatic aberrations using channel alignment information created earlier. The output images are then saved in the proprietary *.czi file format. The average final image resolution was calculated to be 110 nm in x and y dimensions and 240nm in the z dimension, which represents a slightly better than two-fold lateral and axial improvement in resolution, compared to conventional microscopy. Final images can be further analysed in additional software packages. We use Volocity 6.3 software (Perkin Elmer Cell Imaging, Seer Green,

UK) to generate final 3D isosurface renderings and videos of selected cropped regions of the image volumes for presentation and publication. Note that this rendering type means that vesicles positive for green and red do not look yellow but have green and red on the surface (Figure 3).

5. Concluding Remarks

Visualizing PI(5)P and interfering with its metabolism during autophagy represents a new tool to monitor and study autophagosome formation. Although will be important to develop new and more specific PI(5)P probes as well as continue to identify additional effectors to better understand PI(5)P function in autophagy, our approach is employable for screening regulators of autophagy.

Acknowledgements

We are grateful to the Wellcome Trust (Principal Research Fellowship to DCR (095317/Z/11/Z)) and a Strategic Grant to Cambridge Institute for Medical Research (100140/Z/12/Z) for funding.

References

Alvarez-Venegas, R., M. Sadder, A. Hlavacka, F. Baluska, Y. Xia, G. Lu, A. Firsov, G. Sarath, H. Moriyama, J. G. Dubrovsky and Z. Avramova (2006). "The Arabidopsis homolog of trithorax, ATX1, binds phosphatidylinositol 5-phosphate, and the two regulate a common set of target genes." Proc Natl Acad Sci U S A **103**(15): 6049-6054.

Balla, T. (2013). "Phosphoinositides: tiny lipids with giant impact on cell regulation." Physiol Rev **93**(3): 1019-1137.
Baskaran, S., M. J. Ragusa, E. Boura and J. H. Hurley (2012). "Two-site recognition of phosphatidylinositol 3-phosphate by PROPPINs in autophagy." Mol Cell **47**(3): 339-348.
Boal, F., R. Mansour, M. Gayral, E. Saland, G. Chicanne, J. M. Xuereb, M. Marcellin, O. Burlet-Schiltz, P. J. Sansonetti, B. Payrastre and H. Tronchere (2015). "TOM1 is a PI5P effector involved in the regulation of endosomal maturation." J Cell Sci **128**(4): 815-827.
Bua, D. J., G. M. Martin, O. Binda and O. Gozani (2013). "Nuclear phosphatidylinositol-5-phosphate regulates ING2 stability at discrete chromatin targets in response to DNA damage." Sci Rep **3**: 2137.
Chen, B. C., W. R. Legant, K. Wang, L. Shao, D. E. Milkie, M. W. Davidson, C. Janetopoulos, X. S. Wu, J. A. Hammer, 3rd, Z. Liu, B. P. English, Y. Mimori-Kiyosue, D. P. Romero, A. T. Ritter, J. Lippincott-Schwartz, L. Fritz-Laylin, R. D. Mullins, D. M. Mitchell, J. N. Bembenek, A. C. Reymann, R. Bohme, S. W. Grill, J. T. Wang, G. Seydoux, U. S. Tulu, D. P. Kiehart and E. Betzig (2014). "Lattice light-sheet microscopy: imaging molecules to embryos at high spatiotemporal resolution." Science **346**(6208): 1257998.
Clarke, J. H., M. Wang and R. F. Irvine (2010). "Localization, regulation and function of type II phosphatidylinositol 5-phosphate 4-kinases." Adv Enzyme Regul **50**(1): 12-18.
Codogno, P., M. Mehrpour and T. Proikas-Cezanne (2012). "Canonical and non-canonical autophagy: variations on a common theme of self-eating?" Nat Rev Mol Cell Biol **13**(1): 7-12.
Dall'Armi, C., K. A. Devereaux and G. Di Paolo (2013). "The role of lipids in the control of autophagy." Curr Biol **23**(1): R33-45.
Di Lello, P., B. D. Nguyen, T. N. Jones, K. Potempa, M. S. Kobor, P. Legault and J. G. Omichinski (2005). "NMR structure of the amino-terminal domain from the Tfb1 subunit of TFIIH and characterization of its phosphoinositide and VP16 binding sites." Biochemistry **44**(21): 7678-7686.
Fugier, C., A. F. Klein, C. Hammer, S. Vassilopoulos, Y. Ivarsson, A. Toussaint, V. Tosch, A. Vignaud, A. Ferry, N. Messaddeq, Y. Kokunai, R. Tsuburaya, P. de la Grange, D. Dembele, V. Francois, G. Precigout, C. Boulade-Ladame, M. C. Hummel, A. Lopez de Munain, N. Sergeant, A. Laquerriere, C. Thibault, F. Deryckere, D. Auboeuf, L. Garcia, P. Zimmermann, B. Udd, B. Schoser, M. P. Takahashi, I. Nishino, G. Bassez, J. Laporte, D. Furling and N. Charlet-Berguerand (2011). "Misregulated alternative splicing of BIN1 is associated with T tubule alterations and muscle weakness in myotonic dystrophy." Nat Med **17**(6): 720-725.
Gelato, K. A., M. Tauber, M. S. Ong, S. Winter, K. Hiragami-Hamada, J. Sindlinger, A. Lemak, Y. Bultsma, S. Houliston, D. Schwarzer, N. Divecha, C. H. Arrowsmith and W. Fischle (2014). "Accessibility of different histone H3-binding domains of UHRF1 is allosterically regulated by phosphatidylinositol 5-phosphate." Mol Cell **54**(6): 905-919.
Gozani, O., P. Karuman, D. R. Jones, D. Ivanov, J. Cha, A. A. Lugovskoy, C. L. Baird, H. Zhu, S. J. Field, S. L. Lessnick, J. Villasenor, B. Mehrotra, J. Chen, V. R. Rao, J. S. Brugge, C. G. Ferguson, B. Payrastre, D. G. Myszka, L. C. Cantley, G. Wagner, N. Divecha, G. D. Prestwich and J. Yuan (2003). "The PHD finger of the chromatin-associated protein ING2 functions as a nuclear phosphoinositide receptor." Cell **114**(1): 99-111.

Grindheim, A. K., H. Hollas, J. Ramirez, J. Saraste, G. Trave and A. Vedeler (2014). "Effect of serine phosphorylation and Ser25 phospho-mimicking mutations on nuclear localisation and ligand interactions of annexin A2." J Mol Biol **426**(13): 2486-2499.
Guittard, G., A. Gerard, S. Dupuis-Coronas, H. Tronchere, E. Mortier, C. Favre, D. Olive, P. Zimmermann, B. Payrastre and J. A. Nunes (2009). "Cutting edge: Dok-1 and Dok-2 adaptor molecules are regulated by phosphatidylinositol 5-phosphate production in T cells." J Immunol **182**(7): 3974-3978.
Guittard, G., E. Mortier, H. Tronchere, G. Firaguay, A. Gerard, P. Zimmermann, B. Payrastre and J. A. Nunes (2010). "Evidence for a positive role of PtdIns5P in T-cell signal transduction pathways." FEBS Lett **584**(11): 2455-2460.
Gustafsson, M. G., L. Shao, P. M. Carlton, C. J. Wang, I. N. Golubovskaya, W. Z. Cande, D. A. Agard and J. W. Sedat (2008). "Three-dimensional resolution doubling in wide-field fluorescence microscopy by structured illumination." Biophys J **94**(12): 4957-4970.
Hammond, G. R. and T. Balla (2015). "Polyphosphoinositide binding domains: Key to inositol lipid biology." Biochim Biophys Acta **1851**(6): 746-758.
Ikonomov, O. C., D. Sbrissa, K. Delvecchio, Y. Xie, J. P. Jin, D. Rappolee and A. Shisheva (2011). "The phosphoinositide kinase PIKfyve is vital in early embryonic development: preimplantation lethality of PIKfyve-/- embryos but normality of PIKfyve+/- mice." J Biol Chem **286**(15): 13404-13413.
Jones, M. and N. Smirnoff (2006). "Nuclear dynamics during the simultaneous and sustained tip growth of multiple root hairs arising from a single root epidermal cell." J Exp Bot **57**(15): 4269-4275.
Liu, H., Z. Q. Liu, C. X. Chen, S. Magill, Y. Jiang and Y. J. Liu (2006). "Inhibitory regulation of EGF receptor degradation by sorting nexin 5." Biochem Biophys Res Commun **342**(2): 537-546.
Lorenzo, O., S. Urbe and M. J. Clague (2005). "Analysis of phosphoinositide binding domain properties within the myotubularin-related protein MTMR3." J Cell Sci **118**(Pt 9): 2005-2012.
McAlpine, F., L. E. Williamson, S. A. Tooze and E. Y. Chan (2013). "Regulation of nutrient-sensitive autophagy by uncoordinated 51-like kinases 1 and 2." Autophagy **9**(3): 361-373.
McCartney, A. J., Y. Zhang and L. S. Weisman (2014). "Phosphatidylinositol 3,5-bisphosphate: low abundance, high significance." Bioessays **36**(1): 52-64.
Niebuhr, K., S. Giuriato, T. Pedron, D. J. Philpott, F. Gaits, J. Sable, M. P. Sheetz, C. Parsot, P. J. Sansonetti and B. Payrastre (2002). "Conversion of PtdIns(4,5)P(2) into PtdIns(5)P by the S.flexneri effector IpgD reorganizes host cell morphology." EMBO J **21**(19): 5069-5078.
Ozaki, S., D. B. DeWald, J. C. Shope, J. Chen and G. D. Prestwich (2000). "Intracellular delivery of phosphoinositides and inositol phosphates using polyamine carriers." Proc Natl Acad Sci U S A **97**(21): 11286-11291.
Pankiv, S., E. A. Alemu, A. Brech, J. A. Bruun, T. Lamark, A. Overvatn, G. Bjorkoy and T. Johansen (2010). "FYCO1 is a Rab7 effector that binds to LC3 and PI3P to mediate microtubule plus end-directed vesicle transport." J Cell Biol **188**(2): 253-269.
Proikas-Cezanne, T., Z. Takacs, P. Donnes and O. Kohlbacher (2015). "WIPI proteins: essential PtdIns3P effectors at the nascent autophagosome." J Cell Sci **128**(2): 207-217.
Rameh, L. E., K. F. Tolias, B. C. Duckworth and L. C. Cantley (1997). "A new pathway for synthesis of phosphatidylinositol-4,5-bisphosphate." Nature **390**(6656): 192-196.

Ramel, D., F. Lagarrigue, V. Pons, J. Mounier, S. Dupuis-Coronas, G. Chicanne, P. J. Sansonetti, F. Gaits-Iacovoni, H. Tronchere and B. Payrastre (2011). "Shigella flexneri infection generates the lipid PI5P to alter endocytosis and prevent termination of EGFR signaling." Sci Signal **4**(191): ra61.
Ravikumar, B., K. Moreau, L. Jahreiss, C. Puri and D. C. Rubinsztein (2010). "Plasma membrane contributes to the formation of pre-autophagosomal structures." Nat Cell Biol **12**(8): 747-757.
Rubinsztein, D. C., P. Codogno and B. Levine (2012). "Autophagy modulation as a potential therapeutic target for diverse diseases." Nat Rev Drug Discov **11**(9): 709-730.
Sarkes, D. and L. E. Rameh (2010). "A novel HPLC-based approach makes possible the spatial characterization of cellular PtdIns5P and other phosphoinositides." Biochem J **428**(3): 375-384.
Sbrissa, D., O. C. Ikonomov, C. Filios, K. Delvecchio and A. Shisheva (2012). "Functional dissociation between PIKfyve-synthesized PtdIns5P and PtdIns(3,5)P2 by means of the PIKfyve inhibitor YM201636." Am J Physiol Cell Physiol **303**(4): C436-446.
Sbrissa, D., O. C. Ikonomov and A. Shisheva (2002). "Phosphatidylinositol 3-phosphate-interacting domains in PIKfyve. Binding specificity and role in PIKfyve. Endomenbrane localization." J Biol Chem **277**(8): 6073-6079.
Shisheva, A. (2013). "PtdIns5P: news and views of its appearance, disappearance and deeds." Arch Biochem Biophys **538**(2): 171-180.
Stijf-Bultsma, Y., L. Sommer, M. Tauber, M. Baalbaki, P. Giardoglou, D. R. Jones, K. A. Gelato, J. van Pelt, Z. Shah, H. Rahnamoun, C. Toma, K. E. Anderson, P. Hawkins, S. M. Lauberth, A. P. Haramis, D. Hart, W. Fischle and N. Divecha (2015). "The basal transcription complex component TAF3 transduces changes in nuclear phosphoinositides into transcriptional output." Mol Cell **58**(3): 453-467.
Vergne, I. and V. Deretic (2010). "The role of PI3P phosphatases in the regulation of autophagy." FEBS Lett **584**(7): 1313-1318.
Viaud, J., F. Boal, H. Tronchere, F. Gaits-Iacovoni and B. Payrastre (2013). "Phosphatidylinositol 5-phosphate: A nuclear stress lipid and a tuner of membranes and cytoskeleton dynamics." Bioessays.
Viaud, J., F. Boal, H. Tronchere, F. Gaits-Iacovoni and B. Payrastre (2014). "Phosphatidylinositol 5-phosphate: a nuclear stress lipid and a tuner of membranes and cytoskeleton dynamics." Bioessays **36**(3): 260-272.
Viaud, J., F. Lagarrigue, D. Ramel, S. Allart, G. Chicanne, L. Ceccato, D. Courilleau, J. M. Xuereb, O. Pertz, B. Payrastre and F. Gaits-Iacovoni (2014). "Phosphatidylinositol 5-phosphate regulates invasion through binding and activation of Tiam1." Nat Commun **5**: 4080.
Vicinanza, M., V. I. Korolchuk, A. Ashkenazi, C. Puri, F. M. Menzies, J. H. Clarke and D. C. Rubinsztein (2015). "PI(5)P regulates autophagosome biogenesis." Mol Cell **57**(2): 219-234.
Viiri, K. M., J. Janis, T. Siggers, T. Y. Heinonen, J. Valjakka, M. L. Bulyk, M. Maki and O. Lohi (2009). "DNA-binding and -bending activities of SAP30L and SAP30 are mediated by a zinc-dependent module and monophosphoinositides." Mol Cell Biol **29**(2): 342-356.
Zhou, X., L. Wang, H. Hasegawa, P. Amin, B. X. Han, S. Kaneko, Y. He and F. Wang (2010). "Deletion of PIK3C3/Vps34 in sensory neurons causes rapid neurodegeneration by disrupting the endosomal but not the autophagic pathway." Proc Natl Acad Sci U S A **107**(20): 9424-9429.

Zolov, S. N., D. Bridges, Y. Zhang, W. W. Lee, E. Riehle, R. Verma, G. M. Lenk, K. Converso-Baran, T. Weide, R. L. Albin, A. R. Saltiel, M. H. Meisler, M. W. Russell and L. S. Weisman (2012). "In vivo, Pikfyve generates PI(3,5)P2, which serves as both a signaling lipid and the major precursor for PI5P." Proc Natl Acad Sci U S A **109**(43): 17472-17477.

Figure legends

Figure 1: (**a**) Autophagy pathways regulated by PI(5)P (Vicinanza, Korolchuk et al. 2015); (**b**) Summary of cellular proteins shown to bind PI(5)P by different lipid interaction domains and localized in diverse subcellular compartments. PH, Pleckstrin homology domain, PHD, plant homeo-domain, PH-GRAM (Glucosyl transferase, Rab-like GTPase activator and Myotubularins), PBR (PolyBasicRegion), VHS (Vps27-Hrs-STAM). Note that some of these proteins (i.e. WIPI1 and WIPI2) have been shown to bind PI(3)P and PI(3,5)P2. (**c**) Schematic representation of pathways for PI(5)P and PI(3)P synthesis/turnover and compounds targeting enzymes involved in these pathways.

Figure 2: (**a**) Maximum image resolution of Super Resolution Structured Illuminated microscopy (SR-SIM) and conventional confocal microscopy; (**b**) Zeiss Elyra PS1 microscope equipped with an environment-controlled chamber; (**c**) Image acquisition and image processing of Super Resolution Structured Illuminated microscopy (SR-SIM) and conventional confocal microscopy.

Figure 3: HeLa cells transfected with GFP-PHD3X and Strawberry-ATG16L1 for 16 h were left in HBSS for 1h, then fixed and imaged on Elyra superresolution microscope (Vicinanza, Korolchuk et al. 2015). Final visualisation was performed in Volocity 6.3 Software using maximum intensity projection (left) or iso-surface rendering (right) of selected cropped regions of the datasets. Note that when rendering is applied, vesicles that are positive for green and red, have green and red on the surface but do not appear yellow (as showed maximum intensity projection on the left). It is inherently difficult to present such 3D data in a 2D format. Usually such data are presented via maximum intensity projection (MIP) which we have also

shown on the left. We felt that MIP rendering was insufficient in this case to properly appreciate the shapes of the structures presented. To improve matters, we chose to use iso-surface rendering, which uses light and shade to better present 3D structures as solid forms. The reflected light and shadows are important visual cues, which allow a certain degree of three dimensionality in a 2D reproduction. Of course, the best way to evaluate the structure is to see a movie where the iso-surface image is rotated in space.

a

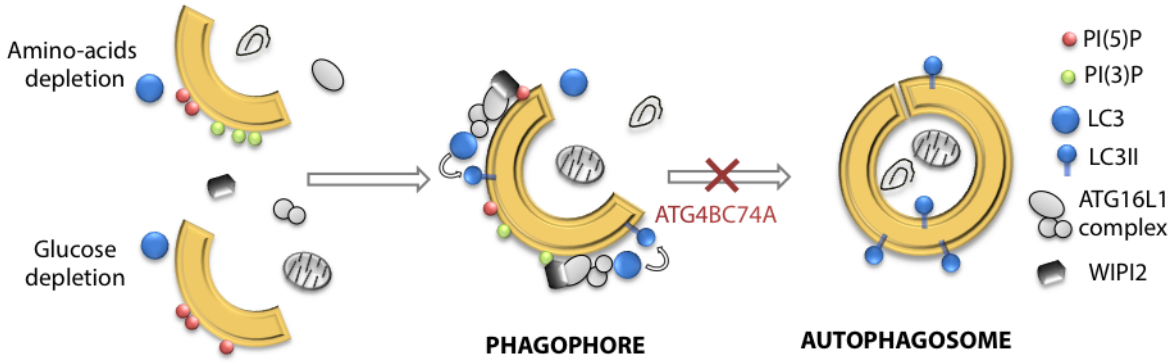

b

PI(5)P binding proteins

Protein	PI binding Domain	Localization	REF
WIPI1, WIPI2	FRRG motif	Autophagosome	Baskaran, 2012, Mol Cell
MTMR3	PH-GRAM	Autophagosome, Golgi	Lorenzo, 2005, JCS
Dok1, Dok2, Dok4, Dok5	PH	Plasma-membrane	Guittard, 2009, Journ Immunol Guittard, 2010, FEBS Lett
BIN1	-	Endosomes	Fugier, 2011, Nature Medicine
TOM1	VHS	Endosomes	Boal, 2015, JCS
TIAM1	PH	Endosomes	Viaud, 2014, Nat Comm
SNX5	-	Endosomes	Liu, 2006, BBRC
Annexin A2	-	Endosomes, plasma membrane, nucleus	Grindheim, 2014, JMB
ING2	PHD	Nucleus	Gozani, 2003, Cell Bua, 2013, Sci Rep
ATX1	PHD	Nucleus	Alvarez-Venegas 2006, PNAS
TFIIH	PH	Nucleus	Di Lello 2005, Biochemistry
Sap30/Sap30L	-	Nucleus	Viiri 2009, MCB
TAF3	PHD	Nucleus	Stijf-Bultsma 2015, Mol Cell
UHRF1	PBR	Nucleus	Gelato 2014, Mol Cell
PLEKHA5	PH	-	Yamada, 2012, Gene

c

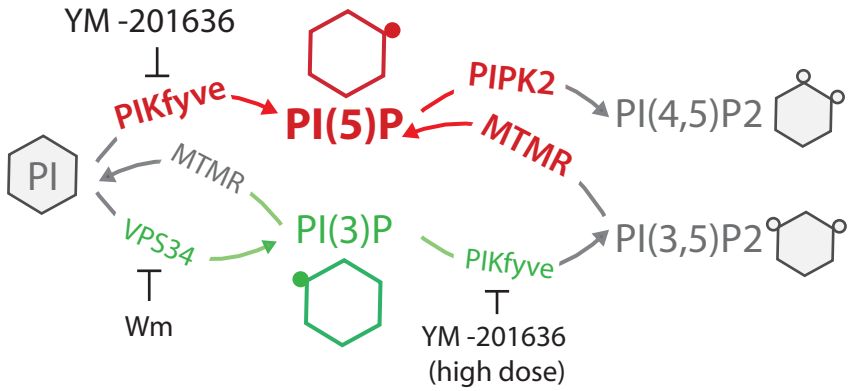

Figure 1

a **Maximum Resolution (GFP) in Confocal Microscopy**

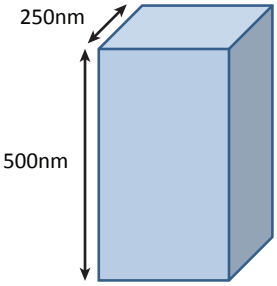

Maximum Resolution (GFP) in SR-SIM

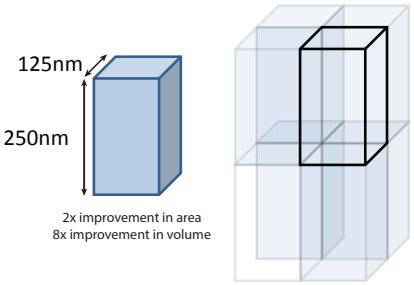

b

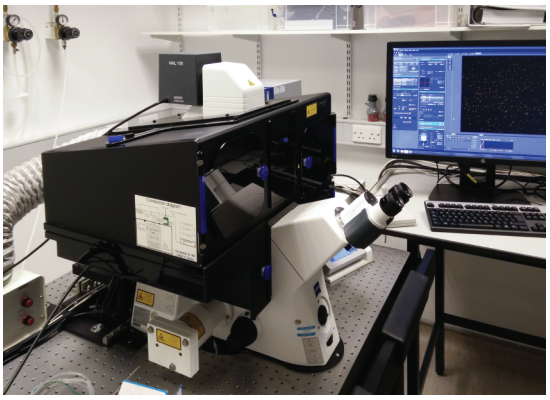

Zeiss Elyra PS1 Microscope with laser safe incubation

c **Confocal Microscopy**

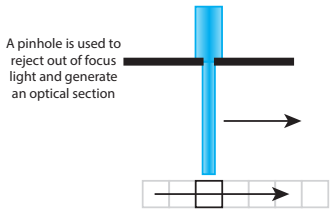

The sample is scanned by a laser point by point to build a 2D or 3D image over time. This process can be moderately quick and is suitable for live samples

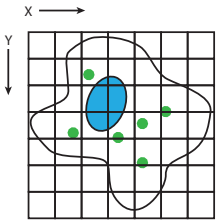

The confocal image is immediately seen and is ready for analysis. It does not require further processing.

The resolution is limited by diffraction and the size of the illumination volume (pixel size is exaggerated for clarity)

Super-Resolution Structured Illumination Microscopy (SR-SIM)

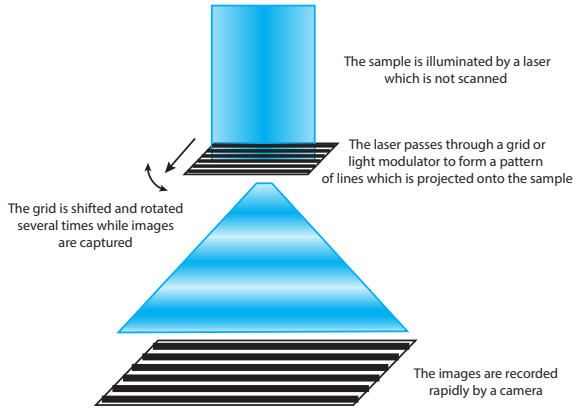

High frequency information is encoded in the interference patterns caused by the grid movements. This information is extracted by post-processing the dataset

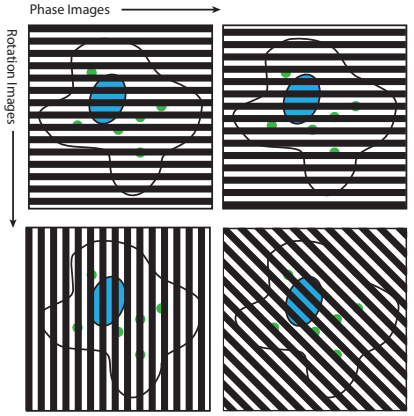

Multiple phase and rotation images are combined and processed into the final image, this takes a lot of computational time

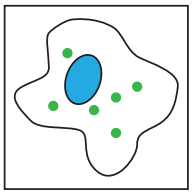

The resolution is no longer limited by diffraction but determined by the number of phase and rotation images and the processing algorithms

Figure 2

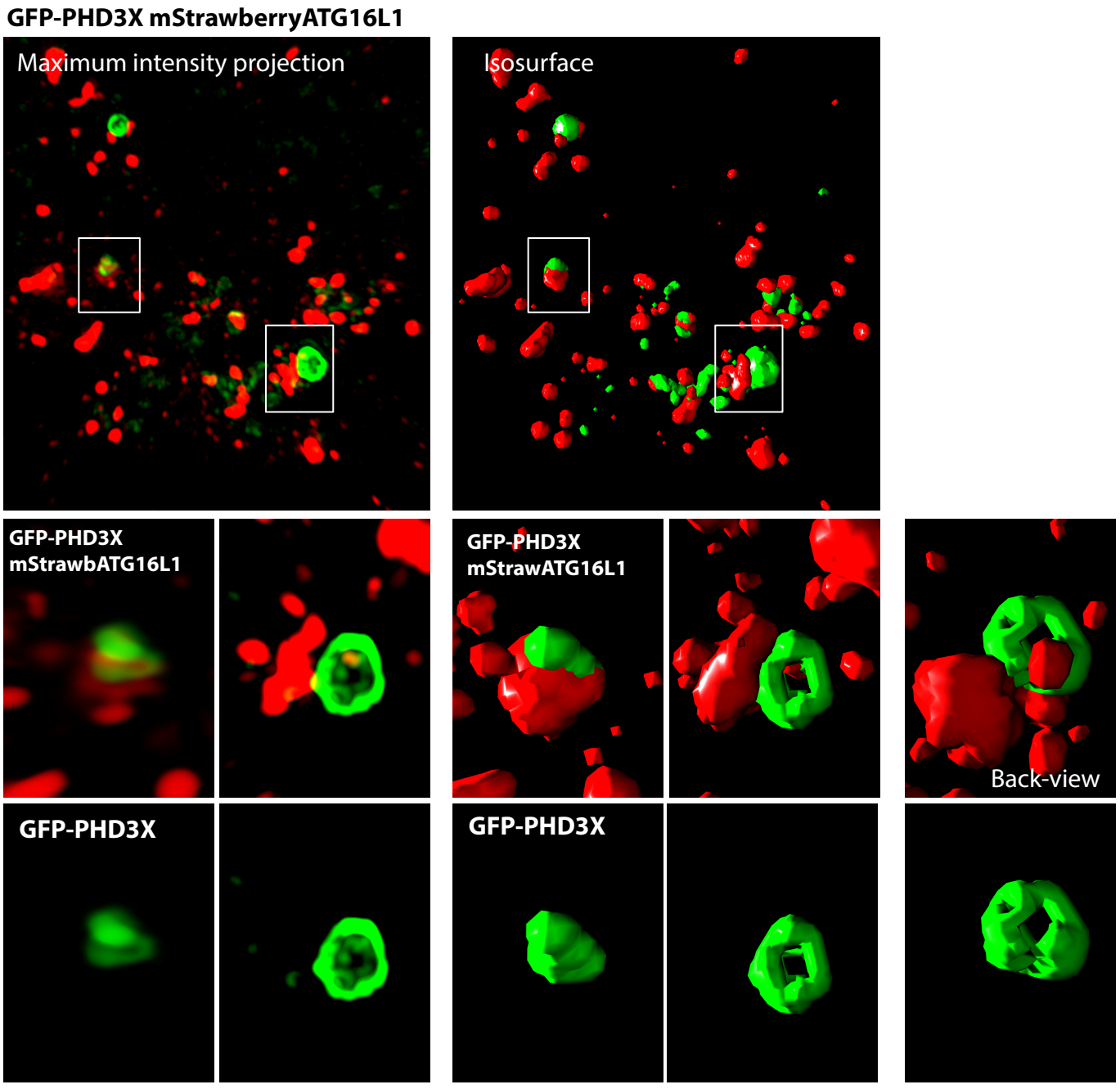
GFP-PHD3X mStrawberryATG16L1
Maximum intensity projection
Isosurface
GFP-PHD3X
mStrawbATG16L1
GFP-PHD3X
mStrawATG16L1
Back-view
GFP-PHD3X
GFP-PHD3X

Figure 3